USE OF SMALL SCALE ELECTRICAL RESISTIVITY TOMOGRAPHY TO IDENTIFY SOIL-ROOT INTERACTIONS DURING DEFICIT IRRIGATION

Vanella D.[1*], Cassiani G.[2], Busato L.[2], Boaga J.[2], Barbagallo S.[1], Binley A.[3], Consoli S.[1]

[1] Dipartimento di Agricoltura, Alimentazione, Ambiente (Di3A), Università degli Studi di Catania, Via S. Sofia, 100 – 95123 Catania (Italy)

[2] Dipartimento di Geoscienze, Università degli Studi di Padova, Via Gradenigo, 6 – 35131 Padova (Italy)

[3] Lancaster Environment Centre, Lancaster University, Lancaster LA1 4YQ (UK)

* corresponding author: d.vanella@unict.it +39 095 7147554

Abstract

Plant roots affect the exchanges of mass and energy between the soil and atmosphere. However, it is challenging to monitor the activity of the root-zone because roots are not visible from the soil surface, and root systems undergo spatial and temporal variations in response to internal and external conditions. Therefore, measurements of the activity of root systems are interesting to plant biologists in general, and are especially important for specific applications, such as precision agriculture. This study demonstrates the use of small scale three-dimensional (3-D) electrical resistivity tomography (ERT) to monitor the root-zone of orange trees irrigated by two different regimes: (i) full rate, in which 100% of the crop evapotranspiration (ET_c) is provided, and (ii) partial root-zone drying (PRD), in which 50% of ET_c is supplied to alternate sides of the tree. We performed time-lapse 3-D ERT measurements on these trees from 5 June to 24 September 2015, and compared the long-term and short-term changes before, during, and after irrigation events. Given the small changes in soil temperature and pore water electrical conductivity, we interpreted changes of soil electrical resistivity from 3-D ERT data as proxies for changes in soil water content. The ERT results are consistent with measurements of transpiration flux and soil temperature. The changes in electrical resistivity obtained from ERT measurements in this case study indicate that

root water uptake (RWU) processes occur at the 0.1 m scale, and highlight the impact of different irrigation schemes.

Keywords: deficit irrigation; geophysical methods; soil-root interactions; soil moisture.

1 Introduction

Root activity plays a crucial role in soil-plant-atmosphere systems because it connects the different domains and facilitates the exchange of water and nutrients necessary for plant growth (Liu et al., 2016; Yang et al., 2016). An assessment of the mass exchange dynamics within the soil-plant system may help to identify the characteristics of the root system that are most important for water uptake (Jayawickreme et al., 2014; Parsekian et al., 2015). This assessment may also have practical implications, in that it could improve of precision agriculture (PA), especially when optimization of water resources is required (Consoli and Papa, 2013).

Geophysical methods (Vereecken et al., 2006; Allred et al., 2008; Binley et al., 2015) are potentially effective for monitoring of soil-root interactions. In particular, the effect of plant growth, phenological stage, nutrient availability, and soil texture on plant root distribution dynamics , combined with the intermittent nature of water inputs, lead to great variability in root water uptake (RWU) (Van Noordwijk et al. 2015). These patterns can be difficult to identify, even when using dense networks of point sensors that measure soil moisture dynamics (Jayawickreme et al., 2008, 2014).

Traditionally, researchers estimated soil moisture content by gravimetric analysis of extracted samples or use of techniques that measure its dielectric properties. These techniques, albeit often accurate, are point measurements, and cannot provide sufficient information on the spatial distribution of state variables for reliable mass balance assessments. Remote sensing techniques generally have limited penetration depth (Robinson et al., 2008). Thus, the interpretation of RWU as a spatially distributed system remains a challenge. In this respect, there is a growing demand for near-surface observing technologies (e.g. geophysical methods) to study agriculturally significant phenomena in the soil (Bitella et al., 2015). Recent studies (Cassiani et al., 2015; Consoli et al., 2017; Satriani et al., 2015) demonstrated that these techniques can improve irrigation operations by providing information regarding the optimal amounts and timing of irrigation. Geophysical methods can also provide indirect high-resolution information on soil moisture distribution, and this can prevent excessive water depletion, especially when water deficit conditions are imposed, such as when using the irrigation technique of partial root-zone drying (PRD) (Romero-Conde et al., 2014). In particular, given the specificity of PRD, geophysical applications may provide identification of changes in soil moisture.

PRD is an irrigation strategy in which half of the root system is in a drying state, and the other half is irrigated; the wet and dry parts are alternated at a frequency that depends on the type of crop, growing stage, and soil water content (Zhang et al., 2001). This strategy may decrease water use and canopy vigor, maintain crop yields because crops take up water from the wet soil zones, and increase crop quality due to changes in abscisic acid (ABA) production (Brillante et al., 2015). Few studies of the magnitude of soil moisture variations in PRD have used geophysical applications. Electrical resistivity tomography (ERT) is considered one of the most effective geophysical methods used in agriculture and environmental studies. This is a minimally-invasive method that provides data with high spatial and temporal resolution (Michot et al. 2003; al Hagrey 2007). More specifically, ERT provides information on the variability of electrical resistivity (ER) of the subsoil; when considered along with water and solute content, it can help to characterize the spatial distribution of water and nutrient uptake (Srayeddin and Doussan, 2009).

Previous researchers have used ERT to observe transient state phenomena in the soil-plant continuum. In particular, these studies used ERT and other electrical techniques to monitor RWU processes of herbaceous crops in the laboratory (Werban et al., 2008) and in the field (Srayeddin and Doussan, 2009; Garré et al., 2011; Beff et al., 2013; Cassiani et al., 2015; Consoli et al., 2017; Whalley et al., 2017), and demonstrated the match between soil water content variations and temporal changes in ER. However, the effects of pore water electrical conductivity (EC) changes and temperature variations (Samouëlian et al., 2005) must also be considered (Cassiani et al., 2016). Soil texture and composition, including the nature of the solid constituents (particle size distribution and mineralogy) and the arrangement of voids (porosity, pore size distribution, and connectivity), can lead to time-invariant heterogeneities in the ER. Thus, a one-to-one relationship between ER and soil moisture content cannot be assumed, and the effect of the other factors must be considered on a case-by-case basis. The variability of these factors must be restricted by use of time-lapse measurements or independent measurements with a calibration equation (Michot et al., 2003).

Michot et al. (2003) used 2-D time-lapse ERT monitoring to identify soil drying patterns in shallow soil, where root activity is more intense (see also Whalley et al., 2017). Other authors used ERT in eco-physiological studies of fruit crops, such as oranges (Cassiani et al., 2015; Moreno et al., 2015), apples (Boaga et al., 2013; Cassiani et al., 2016), olive and poplar trees (al Hagrey, 2007), and natural forests (Nijland et al., 2010; Robinson et al., 2012). Mares et al. (2016) and Wang et al. (2016) recently used ERT on tree trunks to determine cross-sectional water distribution and identify preferential flow into stems through multi-height measurements. However, Brillante et al. (2015) noted that few eco-physiological studies have used ERT in parallel with monitoring of plant water status, and that further investigations are needed to answer new questions about plant-soil relationships, and to increase the use of new techniques for water management in agriculture. These previous studies (Table 1) show the potential of ERT for agricultural applications, even though difficulties remain in the interpretation of measured ER patterns, especially in field settings. The major difficulties are that ER is a function of a number of soil properties and state variables (as noted above) and that rapid changes in the soil-plant-atmosphere continuum, such as passage of an infiltration front after irrigation and/or a heavy rainfall, require measurements with high temporal resolution to avoid aliasing (Koestel et al., 2009). Finally, RWU processes have high spatial variability, and require a resolution of at least 0.1 m (Michot et al., 2003).

< *Table 1 here please* >

In this study, we performed 3-D ERT time-lapse monitoring of heterogeneous sites in an orange orchard to:

i. Verify the reliability of a small scale ERT setup to qualitatively monitor the soil-root interaction in the presence of two irrigation treatments—full drip irrigation *vs.* partial root-zone drying—at different time scales;
ii. Identify the active RWU patterns and their time evolution, by integrating time-lapse ERT data with ancillary measurements for the different water treatments.

2 Materials and Methods

2.1 Experimental site and irrigation scheduling

We conducted small scale 3-D ERT monitoring in an orange orchard (*Citrus sinensis* (L.) Osbeck) in Eastern Sicily, Italy (37°20' N, 14°53' E, Figure 1) during the 2015 irrigation season (5 June to 24 September). The grove belongs to the Citrus and Mediterranean Crops Research Centre of the Italian Council for Agricultural Research and Agricultural Economics Analyses (CREA-ACM, Acireale, Sicily). The trees were 8 years-old, 4 m apart within rows, 6 m apart between rows, (Figure 2), had a mean leaf area index (LAI) of 4.5 m^2 m^{-2}, and mean PAR light interception of 75% (Consoli et al., 2017). The climate parameters at the experimental site (global radiation, relative humidity, wind speed and direction, air temperature) were measured and logged hourly using an automatic meteorological station (Siap and Micros s.r.l.), which was installed 15 m from the experimental orchard and surrounded by grass (according to Central Office of Agricultural Ecology-UCEA procedure). The climate of the region is semi-arid Mediterranean, with warm and dry summers. The study period was fairly dry, with total rainfall of about 100 mm (from a few episodic events). The crop reference evapotranspiration rate (ET_0, Allen et al. 1998) was 697 mm;

the average daily temperature was about 25°C (±5.8°C), and the relative humidity was 70% (±26%). The maximum daily temperature at the experimental site occasionally reached 40°C during the monitoring period.

< *Figure 1 here please* >

The soil is fairly uniform in the top 0.1 m, consisting of a sandy-loam texture (69.7% sand, 10.5% of clay, and 19.8% of silt) and a small percentage of organic matter (1.25%). The mean water content at field capacity (FC, pF = 2.5) was 28% and the mean wilting point (WP, pF = 4.2) was 14%. The bulk density was 1.32 g cm^{-3} (Aiello et al., 2014). Further analyses of soil texture and bulk density were conducted on samples collected at depths of 0.2, 0.4, and 1.0 m. The irrigation water had medium salinity (EC_{25}°C of 2.02 dS m^{-1}), an alkaline reaction, and a pH of 7.30.

Irrigation rates were determined by crop evapotranspiration (ET_c) and adjusted according to rainfall. ET_c was calculated by multiplying ET_0 (obtained from the Penman-Monteith equation (Allen et al., 1998; Allen et al., 2006) by the seasonal crop coefficient (K_c) for orange orchards (0.7 according to FAO-56). The ET_c was further adjusted using a reduction coefficient (0.68), which depends on canopy size with respect to the area of each tree (Consoli et al., 2014). From 5 Jun to 24 Sep 2015, irrigation was supplied to the orchard early in the morning, 3 times per week. Two different irrigation regimes were tested (Figure 2): (i) a control treatment (T1), in which trees received sufficient water to replace 100% of the ET_c, and (ii) a partial root-zone drying treatment (PRD, T2), in which trees received 50% of the ET_c on alternate sides of the root-zone. All trees in T1 and T2 were drip irrigated using two lateral surface pipes (about 0.3 m from the trunk) per tree row; each lateral consisted of six 4 L h^{-1} drippers (spaced 0.62 m apart) per tree. Irrigation in T2 was applied only to one lateral pipe, and the system was switched to the other fortnightly. At the end of the irrigation season, the total irrigation water applied to T1 was 266.4 mm, and that applied to T2 was 158.2 mm, a 41% difference.

The changes in soil water content (SWC; m^3 m^{-3}) were monitored using soil moisture sensors (ECH_2O probe, Decagon, Inc.), which were calibrated in the laboratory using the gravimetric method. Sensors were installed at a depth of 0.3 m from the soil surface in T1 and T2. In T2, soil moisture probes were installed at the eastern and western sides of each tree's trunk (Figure 2).

Soil temperature was measured using thermocouple probes (TVAC, Campbell Sci.) that were placed 0.1 and 0.8 m below the soil surface (Figure 2). If necessary, temperature changes were monitored to correct for their effect on ER.

< Figure 2 here please >

The EC of soil pore water was monitored to evaluate its effect on the changes in soil ER, and to make corrections if needed. In particular, pore water in T1 and T2 was extracted using ceramic suction lysimeters (Soil Solution Access Tube, SSAT by IRROMETER Company, Inc.) installed at a depth of 0.3 m (Figure 3). The EC of the pore water was then measured in the laboratory using an HD2106.2 conductivity meter (delta OHM, Italy). The EC of irrigation water from wells and drip lines was also monitored (Table 2).

< Table 2 here please >

2.1.1 Tree transpiration measurements

Water consumption at the individual tree level was continuously monitored using the heat pulse velocity sap flow technique (HPV, Swanson and Whitfield, 1981). Tree transpiration was measured on 2 trees in T1 and 2 trees in T2. This technique consists of measuring the temperature variation produced by a 1-2 s heat pulse at two temperature probes positioned orthogonally, on either side of a linear heater that was inserted into the trunk to a depth of approximately 0.1 m. In particular, one 4 cm probe with 2 thermocouples (Tranzflo NZ Ltd., Palmerston North, NZ) was positioned in the trunk of each tree. The probe was oriented on the southern side of the trunk, 20 cm from the ground, and wired to a data-logger (CR1000, Campbell Sci., USA) used for heat-pulse control and measurements at sampling intervals of 30 min. The temperature measurements were obtained from ultra-thin thermocouples that were placed 5 and 15 mm into the trunk. Data were processed, as described by Green et al. (2003), to estimate transpiration from an integration of sap flow velocity over sapwood area. Specifically, the volume per unit time of sap flow in a tree stem was estimated by multiplying the sap flow velocity by the cross sectional area of conducting tissue. For this purpose, the fraction of wood ($F_M = 0.48$) and of water ($F_L = 0.33$) in the sapwood was determined on trees in which sap flow probes were installed. In particular, F_M and F_L were measured in wood samples (5 mm diameter, 40 mm length) taken with an increment borer near the probe sets. The calculation of F_M and F_L requires measurements of fresh weight, oven-dried weight, and immersed weight (Si et al., 2009). A wound-effect correction (Green et al. 2003; Motisi et al., 2012; Consoli and Papa, 2013) was used on a per-tree basis. Table 3 summarizes the main manufacturing characteristics of the sensors used in this study.

< Table 3 here please >

2.2 3-D ERT time-lapse monitoring

2.2.1 ERT acquisition scheme

Small scale 3-D ERT monitoring of the soil was conducted near 2 orange trees in T1 and 2 trees in T2 (Figure 2). The 3-D ERT set-up (Figure 3) was an expanded version of previously tested schemes (Boaga et al., 2013; Cassiani et al., 2015, 2016), and used surface and buried electrodes (204 total), so there was a three-dimensional arrangement of electrodes around each tree. For each tree, the setup consists of 9 boreholes (1.2 m deep, green circles in Figure 3), each housing 12 electrodes (vertically spaced at 0.1 m), plus 96 surface electrodes (spaced at 0.26 m on a regular square grid). The boreholes were spaced 1.3 m apart on a square grid, thus delimiting 4 quarters (q1, q2, q3, and q4), one of which (q4) was centered at the tree. Each quarter represents the minimal unit of 3-D ERT acquisition, with 72 electrodes, and surrounded a soil area of about 1.3 m × 1.3 m at a depth of 1.2 m.

< *Figure 3 here please* >

The measurements were performed in an attempt to determine long-term variations (with an irrigation season) and short-term variations (within a day) during the entire irrigation season (5 Jun to 24 Sep 2015). The 3-D ERT long-term monitoring, using all 204 electrodes (Figure 3), was conducted at the following times:

- First ERT monitoring period: 8-10 June 2015, when no irrigation was supplied;
- Second ERT monitoring period: 14-17 July 2015, 1 month after onset of irrigation;
- Third ERT monitoring period: 21-24 September 2015, at the end of irrigation.

At the beginning of each ERT monitoring period, one ERT acquisition was conducted on the full 204 electrode setup (Table 4) and used as the “background” dataset for the short-term time-lapse data.

< *Table 4 here please* >

During the second and third monitoring periods, there was full acquisition of data from all four quarters of T1 and T2 at the end of irrigation. The complexity of the time-lapse processes, due to irrigation and water redistribution, required more frequent data acquisition. Thus, hourly ER data on q4 were recorded for T1 and T2 (Cassiani et al., 2015, 2016) (Table 5).

< *Table 5 here please* >

2.2.2 3-D ERT data processing and inversion

The acquisition procedure described above produced 48 independent datasets, each based on data from 72 electrodes: 40 datasets were from long-term monitoring, including the acquisitions before and after irrigation (see Table 4); 8 dataset were from the hourly time-lapse data (Table 5).

All data were acquired using a ten-channel resistivity meter (Syscal Pro 72 Switch, IRIS Instruments) and the same acquisition scheme. In particular, a complete skip-zero dipole-dipole pattern was used, in which the current dipoles and potential dipoles are both of minimal size, because they consist of neighboring electrodes along the boreholes or at the surface. Direct and reciprocal resistance data were acquired to estimate measurement errors (Binley et al., 1995; Daily et al., 2004). In each quarter (72 electrodes), nearly 5000 resistance measurement were acquired, including direct measurements and reciprocals, and each quarter survey lasted 25 min. The pulse duration was 250 ms per measurement cycle, and the target voltage was 50 mV for the current injection. The contact resistances of the electrodes were checked to ensure their suitability for injection of current and accurate measurement of potential differences. Most of the electrodes had excellent contact with the ground (i.e. contact resistance was always less than 5 kΩ), even when the soil was relatively dry.

To produce the inverted resistivity 3-D images, we used the R3t code (Binley, 2013). Unstructured tetrahedral meshes were generated using Gmsh (http://geuz.org/gmsh/, Geuzaine and Remacle, 2009). The data collected (Table 4) were inverted to consider all 4 quarters in the same inversion scheme. The short-term time-lapse data (Table 5) were inverted using only the 72 electrodes surrounding q4.

The strategy used for ERT data processing and inversion consisted of:

1. Reciprocal error identification (i.e. calculation of the error between direct and reciprocal measurements of resistance) (Binley et al., 1995);
2. Inversion of resistance data using Occam's approach (Binley, 2015), in which the target mismatch between measured and computed resistance data is based on the error estimated in step 1 (above); more specifically, three different inversion strategies were adopted:

2.1. Inversions to produce 3-D ER absolute “background” images (Table 4) in all quarters for both treatments; in this case two error levels (10% and 16%) were used, (see step 1 above). Different error levels at different times may be caused by: (i) a weak signal to noise ratio in the dipole-dipole scheme, particularly when there are large separations between current and potential electrode pairs (Binley and Kemna, 2005). Even though this may not be crucial at the small scale of this application, it may lead to different errors under different soil conditions; (ii) dry soils can produce a vacuum at the soil-root interface (Carminati et al., 2009), and this can produce anomalies in the current signal;

2.2. Inversions to produce images of 3-D ER changes before and after irrigation (daily time scale, Table 4). These relative inversions (“time-lapse resistivity inversions”) are calculated from ratios (d_r, Eq. 1) between the ERT resistances before and after irrigation:

$$d_r = \frac{d_t}{d_0} \cdot F(\sigma_{ohm}) \qquad (1)$$

where d_t and d_0 are the resistance values at time t and time 0 (background), and $F(\sigma_{ohm})$ is the resistance, obtained by running the forward model for an arbitrary conductivity (100 Ω m). This calculation was performed simultaneously for all quarters in T1 and T2 using a 10% error level. The time-lapse resistivity ratio images show changes relative to the reference (initial) value;

2.3. Time-lapse resistivity inversions of the individual quarters containing trees (q4 in Figure 3, Table 5) using the same approach as above, but an error level of 5%.

Note that the error level used in ratio inversion was difficult to estimate, because it is not directly available from the reciprocity check. However, use of about 50% of the error estimated for each of the two datasets in the inversion is common practice (Cassiani et al., 2006), because systematic errors are removed from the time-lapse analysis.

3 Results

3.1 Ancillary data observed during the 3-D ERT monitoring

Figure 4 shows the irrigation rates for T1 and T2 (eastern and western sides of the root apparatus), and the timing of 3-D ERT measurements during the June-September 2015 study period. The SWC (m^3 m^{-3}) results (see Figure 2 for locations of sensors) for the PRD treatment (Figure 4) show the expected alternating drying and wetting cycles on opposite sides of the tree. The results for the T1 treatment show that the SWC remained close to field capacity (FC, 0.28 m^3 m^{-3}).

< Figure 4 here please >

Figure 5 shows the hourly changes in SWC recorded during the 3-D ERT monitoring. The first ERT survey, which was at the beginning of the irrigation season (8-10 Jun 2015; days of the year [DOY]: 159-160, Figure 5a) had SWC values well below the FC for T1 and T2, and the values were close to, and sometimes below, the wilting point (WP, 0.14 m^3 m^{-3}). A rainfall event (effective rainfall: 23 mm) occurred on DOY 160, and this increased the SWC. During the second ERT survey (14-17 Jul 2015, DOY 195-198), one month after the beginning of irrigation, the SWC remained fairly close to the FC for T1. The SWC was slightly lower than the FC for T2 on the west side of the plot (Figure 5b), the region that was irrigated during the prior week (Figure 4), but was higher than the WP on the east side. During the third ERT survey (21-24 Sep 2015, DOY: 264-267), the SWC values were similar on both sides for T2, most likely because the of the high soil moisture (west side: 0.18 m^3 m^{-3}, east side: 0.22 m^3 m^{-3}) at the end of the irrigation season.

< Figure 5 here please >

Average soil temperature variations were approximately 2°C during ERT data acquisition. Considering that ER changes 2% for each 1°C change in temperature (Friedman, 2005), temperature only had a negligible effect on the inferred changes in SWC (Nijland et al., 2010). Figure 6 shows the hourly values of soil temperature recorded at depths of 0.1 m and 0.8 m.

Measurements of soil pore water and irrigation water indicate moderate salinity (Table 2), with EC_{25}°C values in the range of 2-3 dS m^{-1}. These values should not affect the sensitivity of our ERT measurements.

< Figure 6 here please >

During the ERT measurements, the daily average tree transpiration rate was up to 1.9 mm d^{-1} in T1, and 0.9 mm d^{-1} in T2, and the average rate of crop evapotranspiration (ET_c) was 2.1 mm d^{-1}. The transpiration values were fairly steady during the middle of the day (from 12:00 a.m. to 04:00 p.m. LST), most likely due to physiological responses that reduced water losses, such as partial closure of leaf stomata (Motisi et al., 2012).

3.2 Seasonal changes in ERT data

The ERT data had excellent quality, as indicated by the low mean reciprocal errors (T1: 2.6% ± 1%, T2: 2.9% ± 0.9%). Moreover, a large percentage of the data had reciprocity errors below 10%. Most of the ERT inversions converged after 6 to 8 iterations when using a designated error level of 10% to 16%.

Table 4 shows the performance of the inverse model in absolute mode (i.e. resistivity at the beginning of each ERT survey), in terms of the number of iterations needed to reach the solution, amount of data used in the inversion, computational time, number of rejected measurements, and final root mean square (RMS) for an error level of 16%. Most of the data converged after fewer than 5 iterations.

Figure 7 shows the 3-D-electrical resistivity (Ω m) images derived from background acquisitions during June, July, and September of 2015 (Table 4) in T1 (Figure 7a) and T2 (Figure 7b) and the ER profiles, averaged within selected soil layers (0.0-0.2 m; 0.4-0.6 m; 0.6-0.8 m; 0.8-1.0 m; 1.0-1.2 m) of the soil volume for T1 (Figure 7c) and T2 (Figure 7d).

< Figure 7 here please >

Figure 7 indicates that from June to September, the mean ER reduction was from 59 (±31) Ω m to 18 (±4) Ω m in T1, and from 65 (±34) Ω m to 40 (±7) Ω m in T2. These differences reflect differences in irrigation. At the end of the irrigation season (September), the mean reduction of ER in the soil profile (0.0-1.0 m) was 69% in T1 and 38% in T2. The greatest variability of ER was in the shallowest soil layer (0.0-0.2 m), in which the mean resistivity was 118 to 16 Ω m in T1 and 139 to 39 Ω m in T2.

Figure 8 shows box-plot that split the ERT data from June, July, and September into quartiles, and the ER distribution for T1 and T2 at depths of 0.0-0.2 m (Figure 8a and d), 0.4-0.6 m (Figure 8b and e), and 1.0-1.2 m (Figure 8c and f). Application of an analysis of variance (ANOVA) to the ERT dataset indicated no significant differences between the resistivity zones in T1 and T2 at significance levels of 0.05, 0.01, and 0.001.

< Figure 8 here please >

The ER values for T1 decreased regularly around the median from June to September 2015, showing a clear pattern during the irrigation phase (Figures 8a, b, and c). This is in good agreement with distribution of the SWC measurements during the same time (Figures 4 and 5). The ER values for T2 had no clear changes over time, possibly due to the smaller irrigation volume (Figures 8d, e, and f).

3.3 Evidence of RWU patterns from ERT data

Figure 9 shows the time-lapse ratios of ER for T1 (Figure 9a and b) and T2 (Figure 9c and d), relative to background (Figure 7). A value of 100% indicates no change from the background; higher values indicate increases and lower values indicate decreases. Archie's law (1942) and other empirical relationships (Waxman and Smits, 1968; Brovelli and Cassiani, 2011) allow calculation of changes in soil moisture from changes in ER.

< Figure 9 here please >

We also analyzed results in which there were more frequent time-lapse measurements (July and September; Table 5). Figures 10a and 11a show examples of the time-lapse resistivity ratio for q4, and Figures 10b and 11b show the hourly transpiration flux (mm h^{-1}) of the irrigated trees in T1 and T2. On 15 July 2015, at the end of the irrigation (time 03, Table 5), about 40% of the soil volume in q4 (treatment T1, Figure 10a) had a marked decrease in the resistivity ratio, due to progression of the irrigation front. This change in ER decreased from the top soil to the bottom-most layer. The results are the same for the 2 previous time steps in q4 (data not shown). In particular, at time 01 there was decrease in ER of 4% in the soil volume, and at time 02 there was a decrease in ER of 10% in the soil volume (Table 5). Only at the end of irrigation (time 03, Figure 10a), q4 in T1 had an increase ER in 7% of the soil volume. The higher ER values (indicating drier soil) were recorded at depths of 0.6-0.8 m, exactly when plant transpiration was maximal (Figure 10b). Thus, at the spatial and temporal scales used here, the correspondence between ER and transpiration flux increases due to changes in RWU.

< Figure 10 here please >

Figure 11a shows the time-lapse results on 24 September 2015 (time 03) at the end of irrigation (Table 5) for T2. These results indicate a slight decrease of ER in 2-7% of the monitored soil volume at the eastern side (which received irrigation at that time). There were 2 volumes of resistivity changes: (i) at the irrigated eastern side, ER decreased in 22% of the monitored soil volume, mostly in the top 0.4 m, close to the two active drippers. This decline in ER accounted for 5% of the monitored volume at time 01, and 13% at time 02 (Table 5); (ii) at the non-irrigated western side, a slight ER increase of 3% occurred to a depth of 0.4 m. Even in this case, the maximum increase was when plant transpiration was greatest (Figure 11b).

< Figure 11 here please >

4 Discussion

4.1 Seasonal changes in ERT data

Overall, the most notable features of the absolute inversions in Figure 7 are that areas of high resistivity (above 100 Ω m) were most common at depths between 0.4 and 1.0 m at the beginning of the irrigation phase. However, during the irrigation season, these higher ER zones were smaller in magnitude. This is particularly notable in the presence of fairly conductive pore water (2-3 dS m^{-1}) that immediately calls for drier unsaturated conditions to give bulk ER well above 100 Ω m. It is difficult to explain how such highly resistive features can exist at localized depths, without considering that local RWU is reasonably intense at this depth from November to May, when the trees were not irrigated. Only the very small-scale anomalies observed close to the surface, which are smaller than the spatial resolution of our method, can be attributed to inversion artefacts (Kim et al., 2009) or to heterogeneous direct evaporation patterns from the top soil, with soil fracturing in conditions of extreme dryness. At greater depths, water depletion can be attributed to root activity.

One of the most interesting aspects of the patterns of high resistivity (Figure 7) is that they all seem to change substantially over time. This is strong evidence against the wide-spread belief that most of the electrical signals from roots are due to their large lignified structures (Amato et al. 2008; Rossi et al. 2011). In fact, the effect of large roots can be mistaken for the combined effects of strong soil drying that roots exert on nearby soil due to water uptake. Our results seem more consistent with this latter explanation.

4.2 Evidence of RWU patterns from ERT data

The daily time course images (Figure 9) show fairly complex patterns of ER caused by the irrigation and soil moisture depletion from RWU processes (Cassiani et al., 2015, 2016). As for the absolute ER inversions (Figure 7), there is evidence that the activity of the root system was driven by: (i) the need to use irrigation water from June to September, which explains the development of a shallow roots near the drippers, and (ii) the need for the tree to take up water during the non-irrigated period by searching for water deeper in the soil profile.

These patterns of increasing and decreasing ER may be challenging to explain. However, we can interpret some of these phenomena:

- As irrigation occurs in a very localized region of the broader area that is monitored by ERT, it is not surprising that ER tends to decline largely in correspondence to changes at the drippers, creating very consistent patterns that extend from the surface to the bottom of the monitored soil volume (depth of about 1 m);
- Certain areas exhibited increases in ER, irrespective of the application of irrigation water. This is likely because transpiration during the hotter times of the day exceeds the amount of irrigation water, and the corresponding SWC is likely to be lower in the afternoon than early morning. The same effect was observed by Cassiani et al. (2015) in another orange orchard. An unusual characteristic of the results presented here is that some areas of increasing resistivity are at depths where deepest roots occur. In fact, comparison of the higher resistivity zones (Figure 7) with the zones in which resistivity increased (Figure 9) shows a remarkable correspondence;
- The amount of irrigation water was greater for T1 than T2, so the variations in ER tend to be greater in T1, especially during the extreme heat of July, when all the irrigation water in T2 was transpired at nearly all monitored depths.

Our comparison of the hourly ER changes for T1 and T2 indicate 5 key features. First, the resistivity decreases in the soil volume as the irrigation front progresses. Second, the increases of resistivity occur when there are higher transpiration fluxes. Third, greater increases of ER occurred at the drier side of the plot for T2. Fourth, the soil depth that exhibited ER changes was 50% larger in T1 than in T2. Fifth, in general, the finer time resolution provided by single quarter acquisition can help detect processes linked to RWU that modify SWC on an hourly scale, although comparisons of patterns before and after irrigation alone are more difficult to interpret (Figure 9).

Our measurements of the likely RWU distribution should be compared with previous estimates from the literature. Under micro-irrigation (as in our study), orange trees tend to develop shallow root systems, with depths of 0.3 to 0.4 m depending on the soil type (Usman et al., 2016, Iyengar and Shivananda, 1990). A previous study in which there was micro-irrigation of an 8-year old sweet orange (*Citrus sinensis* (L.) Pers.) indicated 70-90% of its active roots were in the top 0.3 m of soil, and at a radial distance of 1.2 m from the trunk (Kotur et al., 1998). Our results indicate that although a large fraction of the RWU area is probably in the top 0.4 m of soil, as also reported by Cassiani et al. (2015) in a similar orchard, there were also deeper RWU areas, particularly before irrigation (based on the high ER patterns in Figure 7); this region remains important during irrigation if there is sufficient water to reach the deeper root structures (Figure 10). In fact, a recent excavation of a 1.3 m-deep soil pit at the site indicated the presence of significant root hair systems at this depth (data not shown).

5 Conclusion

The study documents the effectiveness of the 3-D ERT technique for a small scale application, in which changes in ER are due to changes in soil water. We observed clear patterns of wetting and drying in the soil profiles at seasonal, daily, and hourly time resolutions. These patterns were driven by the irrigation operations and by plant transpiration due to RWU. The 3-D ERT results also indicated that the scale of the quarter plot (about 1.7 m^2) was the minimum needed to capture the main processes at the soil-root interface in our experimental setting. This 3-D ERT study also highlights the complexity of RWU processes, and the need to control for several ancillary ground-based data, including soil temperature, soil pore solution EC, plant transpiration, and soil evaporation. Due to the complexity and heterogeneity of the soil-root system studied here, an integration of hydrological and geophysical modelling might improve the analysis of recorded ER anomalies. Finally, ERT may be considered a useful tool for precision irrigation strategies, in particular for identifying the location of the subsoil where RWU occurs, and may therefore improve the efficiency of irrigation. Future developments of this research should attempt to consider the assimilation of ERT with ancillary measurements into a general hydrological model.

We can make several specific conclusions concerning soil-root processes and monitoring methodology:

- Shallow and deep root zones both appear to be active during different times of the growing season, depending on water availability. This partly contradicts the view that micro-irrigated systems only tend to draw RWU from the shallowest soil layers;
- Electrical resistivity methods are more sensitive to the effects of RWU on soil moisture content, and thus to changes in electrical resistivity over time, than to the ligneous nature of large roots. This is confirmed by the disappearance and appearance of high resistivity patterns in our dataset, a result that is not compatible with the presence of stable, large, and resistive roots;
- Time-intensive monitoring provides more valuable information than occasional measurements conducted under specific transient conditions. This emphasizes the need for permanently installed monitoring systems to record processes at the hourly time scale.

Acknowledgements

The authors wish to thank the four anonymous reviewers and the Associate Editor for their valuable comments and suggestions, which helped to improve an earlier version of this manuscript. We wish to thank Giovanni Zocco and Alessandro Castorina for their support during the geophysical monitoring, and the personnel of the Citrus and Mediterranean Crops Research Centre of the Italian Council for Agricultural Research and Agricultural Economics Analyses (CREA-ACM, Acireale), especially Giancarlo Roccuzzo and Fiorella Stagno. The authors also thank the EU and the Italian Ministry of Education, Universities and Research for funding, as part of the collaborative international consortium IRIDA ("Innovative remote and ground sensors, data and tools into a decision support system for agriculture water management"), financed under the ERA-NET Cofund WaterWorks 2014. This ERA-NET is an integral part of the 2015 Joint Activities developed by the Water Challenges for a Changing World Joint Programme Initiative (Water JPI). The authors also acknowledge support from the ERANET-MED project WASA ("Water Saving in Agriculture: Technological developments for the sustainable management of limited water resources in the Mediterranean area"). G.C., J.B., and L.B. acknowledge funding from the University of Padua project CPDA147114, "Hydro-geophysical monitoring and modelling for the Earth's Critical Zone".

References

Aiello, R., Bagarello, V., Barbagallo, S., Consoli, S. Di Prima, S., Giordano, G., Iovino, M. (2014). An assessment of the Beerkan method for determining the hydraulic properties of a sandy loam soil. Geoderma, 235–236 (2014) 300–307

Al Hagrey, S.A., (2007). Geophysical imaging of root-zone, trunk, and moisture heterogeneity. Journal of Experimental Botany 58: 839–854

Allen, R.G., Pereira, L.S., Raes, D. and Smith, M. (1998). Crop evapotranspiration: guidelines for computing crop requirements. Irrigation and Drainage Paper No. 56. FAO, Rome, Italy

Allen, R.G., Pruitt, W.O., Wright, J.L., Howell, T.H., Ventura, F., Snyder, R., Itenfisu, D., Steduto, P., Berengena, J., Baselga Yrisarry, J., Smith, M., Pereira, L.S., Raes, D., Perrier, A., Alves, I., and Walter, I. 2006. A recommendation on standardized surface resistance for hourly calculation of reference ET_o by the FAO56 Penman-Monteith method. Agricultural Water Management*,* 81, 1-22

Allred B, Daniels JJ, Reza Ehsani M (2008) Handbook of agricultural geophysics. CCR Press, Boca Raton, FL, 410 pp

Amato M., Basso B., Celano G., Bitella G., Morelli G.,Rossi R. (2008). In situ detection of tree root distribution and biomass by multielectrode resistivity imaging. Tree Physiology, 28, 10:1441-1448

Archie, G. E. (1942). The electrical resistivity log as an aid in determining some reservoir characteristics: Petroleum Transactions of American Institute of Mining and Metallurgical Engineers, 146, 54–62.

Beff L, Günther T, Vandoorne B, Couvreur V, Javaux M (2013) Threedimensional monitoring of soil water content in a maize field using electrical resistivity tomography. Hydrology and Earth System Sciences, 17:595–609

Binley, A., Ramirez, A., Daily, W., (1995). Regularised image reconstruction of noisy electrical resistance tomography data. In: Beck, M.S., Hoyle, B.S., Morris, M.A., Waterfall, R.C., Williams, R.A. (Eds.), Process Tomography - 1995. Proceedings of the 4th Workshop of the European Concerted Action on Process Tomography, Bergen, 6–8 April 1995, pp. 401–410

Binley, A.M., and Kemna, A., (2005). DC resistivity and induced polarization methods. In: Rubin Y, Hubbard SS (eds) Hydrogeophysics. Water Sci. Technol. Library, Ser. 50. Springer, New York, pp 129–156

Binley, A., (2013). http://www.es.lancs.ac.uk/people/amb/Freeware/R3t/R3t.htm, R3t software version 1.8 March 2013

Binley, A., (2015). Tools and Techniques: DC Electrical Methods, In: Treatise on Geophysics, 2nd Edition, G Schubert (Ed.), Elsevier., Vol. 11, 233-259, doi:10.1016/B978-0-444-53802-4.00192-5

Binley, A., S. S. Hubbard, J. A. Huisman, A. Revil, D. A. Robinson, K. Singha, and L. D. Slater, (2015). The emergence of hydrogeophysics for improved understanding of subsurface processes over multiple scales, Water Resources Research, 51(6), 3837-3866, DOI: 10.1002/2015WR017016

Bitella, G., Rossi, R., Loperte, A., Satriani, A., Lapenna, V., Perniola, M., & Amato, M. (2015). Geophysical techniques for plant, soil, and root research related to sustainability. In The Sustainability of Agro-Food and Natural Resource Systems in the Mediterranean Basin (pp. 353-372). Springer International Publishing

Boaga, J., Rossi, M., and Cassiani, G., (2013). Monitoring soil-plant interactions in an apple orchard using 3-D electrical resistivity tomography, Conference on Four Decades of Progress in Monitoring and Modeling of Processes in the Soil-Plant-Atmosphere System: Applications and Challenges, Naples, 19–21 June 2013, Procedia Environmental Sciences, 19, 394–402

Brillante, L., Mathieu, O., Bois, B., van Leeuwen, C., Lévêque, J., (2015). The use of soil electrical resistivity to monitor plant and soil water relationships in vineyards. SOIL, 1: 273–286

Brovelli A. and G. Cassiani, 2011, Combined estimation of effective electrical conductivity and permittivity for soil monitoring, Water Resources Research, 47, W08510, doi: 10.1029/2011WR010487, 2011

Carminati, A., Vetterlein, D., Weller, U., Vogel, H. J., Oswald, S. E. (2009). When roots lose contact Vadose Zone J. 8 (2), 805-809, http://dx.doi.org/10.2136/vzj2008.0147

Cassiani, G., V. Bruno, A. Villa, N. Fusi, A.M. Binley (2006). A saline tracer test monitored via time-lapse surface electrical resistivity tomography, *Journal of Applied Geophysics*, 59, 244-259, doi: 10.1016/j.jappgeo2005.10.007

Cassiani, G., Boaga, J., Vanella, D., Perri, M.T., Consoli, S., (2015). Monitoring and modelling of soil-plant root zone interaction: the joint use of ERT, sap flow and Eddy Covariance data to define the volume of an orange tree root zone. Hydrology and Earth System Sciences, 19, 2213-2225, doi: 10.5194/hess-19-2213-2015

Cassiani G, Boaga J, Rossi M, Fadda G, Putti M, Majone B, Bellin A (2016). Soil-plant interaction monitoring: small scale example of an apple orchard in Trentino, North-Eastern Italy. Science of the Total Environment 543: 851-861. doi: 10.1016/j.scitotenv.2015.03.113

Consoli, S., Papa, R., (2013). Corrected surface energy balance to measure and model the evapotranspiration of irrigated orange orchards in semi-arid Mediterranean conditions. Irrigation Science September 2013, Volume 31, Issue 5, pp 1159-1171

Consoli S., Stagno F., Roccuzzo G., Cirelli G. Intrigliolo F. (2014). Sustainable management of limited water resources in a young orange orchard. Agricultural Water Management, Vol. 132, pp. 60-68

Consoli, S., Stagno, F., Vanella, D., Boaga, J., Cassiani, G., & Roccuzzo, G. (2017). Partial root-zone drying irrigation in orange orchards: Effects on water use and crop production characteristics. European Journal of Agronomy, 82, 190-202.

Daily, W.A., Ramirez, A., Binley, A., LaBrecque, D., (2004). Electrical resistivity tomography. Leading Edge 23 (5), 438–442

Friedman, S.P. (2005). Soil properties influencing apparent electrical conductivity: a review. Computers and Electronics in Agriculture 46, 45–70

Garré, S., Javaux, M., Vanderborght, J., Pagès, L., Vereecken, H., (2011). Three-Dimensional Electrical Resistivity Tomography to Monitor Root Zone Water Dynamics. Vadose Zone Journal 10(1):412-424. DOI: 10.2136/vzj2010.0079

Geuzaine, C., & Remacle, J. F. (2009). Gmsh: A 3-D finite element mesh generator with built-in pre-and post-processing facilities. International Journal for Numerical Methods in Engineering, 79(11), 1309-1331

Green S.R.; Clothier, B.; Jardine, B., (2003). Theory and Practical Application of Heat Pulse to Measure Sap Flow. Agronomy Journal, 95, 1371-1379

Iyengar B.R.V., Shivananda T.N. (1990). Root activity pattern in sweet orange citrus sinensis during different seasons. Indian Journal of Agricultural Sciences. 60(9): 605-608

Jayawickreme, D. H., Van Dam, R. L., & Hyndman, D. W. (2008). Subsurface imaging of vegetation, climate, and root-zone moisture interactions. Geophysical Research Letters, 35(18)

Jayawickreme, D. H., Jobbágy, E. G., & Jackson, R. B. (2014). Geophysical subsurface imaging for ecological applications. New Phytologist, 201(4), 1170-1175

Kim, J. H., Yi, M. J., Park, S. G., & Kim, J. G. (2009). 4-D inversion of DC resistivity monitoring data acquired over a dynamically changing earth model. Journal of Applied Geophysics, 68(4), 522-532

Koestel, J., Vanderborght, J., Javaux, M., Kemna, A., Binley, A., and Vereecken, H., (2009). Noninvasive 3-D Transport Characterization in a Sandy Soil Using ERT. Investigating the Validity of ERT-derived Transport Parameters. Vadose Zone J Vol. 8 No. 3, p. 711-722

Kotur, S. C., & Keshava Murthy, S. V. (1998). Root activity distribution studies in citrus, grape, mango and guava using isotopic techniques. Karnataka Journal of Agricultural Science, 11, 651-657

Liu, Q., McVicar, T. R., Yang, Z., Donohue, R. J., Liang, L., & Yang, Y. (2016). The hydrological effects of varying vegetation characteristics in a temperate water-limited basin: Development of the dynamic Budyko-Choudhury-Porporato (dBCP) model. Journal of Hydrology, 543, 595-611

Mares, R., Barnard, H. R., Mao, D., Revil, A., & Singha, K. (2016). Examining diel patterns of soil and xylem moisture using electrical resistivity imaging. Journal of Hydrology, 536, 327-338

Michot, D., Benderitter, Y., Dorigny, A., Nicoullaud, B., King, D.,and Tabbagh, A., (2003). Spatial and temporal monitoring of soil water content with an irrigated corn crop cover using surface electrical resistivity tomography, Water Resources Research, 39, p. 1138

Moreno, Z., Arnon-Zur, A., Furman, A., (2015). Hydro-geophysical monitoring of orchard root zone dynamics in semi-arid region. Irrigation Science, 33:303–318

Motisi, A., Consoli, S., Rossi, F., Minacapilli, M., Cammalleri, C. Papa, R., Rallo, G., D'Urso G. (2012). Eddy covariance and sap flow measurements of energy and mass exchange of woody crops in a Mediterranean environment. Acta Horticolturae 951, 121-127

Nijland, W., Van der Meijde, M., Addink, E. A., & De Jong, S. M. (2010). Detection of soil moisture and vegetation water abstraction in a Mediterranean natural area using electrical resistivity tomography. Catena, 81(3), 209-216

Parsekian, A. D., Singha, K., Minsley, B. J., Holbrook, W. S., & Slater, L. (2015). Multiscale geophysical imaging of the critical zone. Reviews of Geophysics, 53(1), 1-26

Robinson, D. A., Campbell, C. S., Hopmans, J. W., Hornbuckle, B. K., Jones, S. B., Knight, R., ... & Wendroth, O. (2008). Soil moisture measurement for ecological and hydrological watershed-scale observatories: A review. Vadose Zone Journal, 7(1), 358-389

Robinson, J. L.; Slater L. D. Schafer K. V. R., (2012). Evidence for spatial variability in hydraulic redistribution within an oak–pine forest from resistivity imaging. Journal of Hydrology 430–431, 69–79

Romero-Conde, A., Kusakabe, A., & Melgar, J. C. (2014). Physiological responses of citrus to partial rootzone drying irrigation. Scientia Horticulturae, 169, 234-238

Rossi, R. Amato, M., Bitella, G., Bochicchio, R., Ferreira Gomes, J., J., Lovelli, S., Martorella, E., Favale, P., (2011). Electrical resistivity tomography as a non-destructive method for mapping root biomass in an orchard. European Journal of Soil Science, 62 (2), 206–215

Samouëlian A, Cousin I, Tabbagh A, Bruand A, Richard G., (2005). Electrical resistivity survey in soil science: a review. Soil & Tillage Research 83: 173–193

Satriani, A., Loperte, A., Soldovieri, F., (2015). Integrated geophysical techniques for sustainable management of water resource. A case study of local dry bean versus commercial common bean cultivars, Agricultural Water Management, 162, 57-66

Si J, Feng Q, Xi H, Chang Z, Su Y, Zhang K (2009). Sap-flow measurement and scale transferring from sample trees to entire forest stand of Populus euphratica in desert riparian forest in extreme arid region. Sciences in Cold and Arid Regions, 1(3), 258-266

Srayeddin, I. and Doussan, C., (2009). Estimation of the spatial variability of root water uptake of maize and sorghum at the field scale by electrical resistivity tomography, Plant Soil, 319, 185–207, doi: 10.1007/s11104-008-9860-5

Swanson, R.H. and Whitfield, D.W. (1981). A numerical analysis of heat pulse velocity theory and practice. J. Exp. Bot. 32:221-239

Usman, K. M., Muhammad, T., Majid, M., Ali, S. M., Shilan, R., Alireza, M., & Sergey, P. Drip irrigation in Pakistan: status, challenges and future prospects (2016) DOI http://dx. doi. org/10.18551/rjoas. 2016-08.15

Van Noordwijk, M., Lawson, G., Hairiah, K., & Wilson, J. (2015). Root distribution of trees and crops: competition and/or complementarity. Tree–crop interactions, 2nd edition: agroforestry in a changing climate. CAB International, Wallingford, 221-257

Vereecken H, Binley A, Cassiani G, Revil A, Titov K (2006) Applied hydrogeophysics. In: Revil A, Titov K (eds) NATO science series IV: earth and environmental sciences. Springer, Dordrecht, p 383

Yang, Y., Donohue, R. J., & McVicar, T. R. (2016). Global estimation of effective plant rooting depth: Implications for hydrological modeling. Water Resources Research, 52(10), 8260-8276

Wang, H., Guan, H., Guyot, A., Simmons, C. T., & Lockington, D. A. (2016). Quantifying sapwood width for three Australian native species using electrical resistivity tomography. Ecohydrology, 9(1), 83-92

Waxman, M. H., and L. J. M. Smits, 1968, Electrical conductivities in oil-bearing shaly sands, Society of Petroleum Engineering Journal, 8, 107–122

Werban, U., Attia al Hagrey, S., & Rabbel, W. (2008). Monitoring of root-zone water content in the laboratory by 2D geoelectrical tomography. Journal of Plant Nutrition and Soil Science, 171(6), 927-935

Whalley, W.R., Binley, A., Watts, C.W., Shanahan, P., Dodd, I.C., Ober, E.S., Ashton, R.W., Webster, C.P., White, R.P. and Hawkesford, M.J. (2017). Methods to estimate changes in soil water for phenotyping root activity in the field, Plant Soil, 415, 407-422, DOI: 10.1007/s11104-016-3161-1

Zhang, L., Dawes, W. R., & Walker, G. R. (2001). Response of mean annual evapotranspiration to vegetation changes at catchment scale. Water resources research, 37(3), 701-708

Figure captions:

Figure 1: (a) Location of the study site in Sicily (Italy, © 2015 Google); (b) experimental orange orchard; and (c) orange trees at the study site.

Figure 2: Schemes of the irrigation treatments (T1, full drip irrigation; T2, partial root zone drying [PRD]) at the study site, location of sensors for measurement of soil temperature, soil moisture, and tree transpiration, and the small scale ERT installations.

Figure 3: Small scale 3-D ERT monitoring scheme at (a) T1 (b) and T2. The orange circle represents the portion of trees trunks within q4; the black points indicate the locations of the surface and buried electrodes; the blue dotted lines indicate the irrigation pipelines; and the blue circles indicate the suction cups.

Figure 4: Daily changes in soil water content (SWC, $m^3 m^{-3}$) for T1 and T2 from 5 Jun to 24 Sep 2015.

Figure 5: Hourly changes in soil water content (SWC, $m^3 m^{-3}$) during the 3-D ERT monitoring from (a) Jun 8-10, (b), Jul 14-17, and (c) Sep 21-24.

Figure 6: Hourly changes of soil temperature at depths of 0.1 m and 0.8 m during each 3-D ERT monitoring period.

Figure 7: Absolute inversions of background datasets collected during long-term ERT monitoring in 2015 (8-10 Jun, 14-17 Jul, and 21-24 Sep) for (a) T1 and (b) T2 and average electrical resistivity (Ω m) as a function of depth for (c) T1 and (d) T2.

Figure 8: Box-plots of the distribution of ER for (a, b, c) T1 and (d, e, f) T2 at different soil layers.

Figure 9: Time-lapse resistivity ratio for T1 and T2, with correction for background conditions, during (a, c) Jul 2015 and (b, d) Sep 2015.

Figure 10: (a) Change in the resistivity ratio volume at time 03 (after the end of irrigation) relative to time 00 (before irrigation, background) and (b) timing of tree transpiration rate (mm h^{-1}) measurements, irrigation, and ERT measurements. Data are for T1 on 15 Jul 2015.

Figure 11: (a) Change in the resistivity ratio volume at time 03 (after the end of irrigation) relative to time 00 (before irrigation, background) and (b) timing of tree transpiration rate (mm h^{-1}) measurements, irrigation, and ERT measurements. Data are for T2 on 24 Sep 2015.

Table 1: Studies that used ERT to study soil-root interactions (ordered chronologically, then alphabetically), and their specific field applications in relation to the aims of the present study.

Study	Approach/Data	Crop/Location	Irrigation type	Main output related to the present study
Michot et al. 2003	2-D ERT (32 electrodes), SW and thermal profiles	corn crop / Beauce region (France)	full irrigation by sprinkler system	verify ability of ERT to measure changes in soil water dynamics over time (water infiltration and soil drainage by RWU)
Jayawickreme et al 2008	2-D ERT (84 electrodes), capacitance-type SW probes, and temperature profiles	maple forest and grassland / Michigan (USA)		monitor large seasonal changes in root-zone moisture dynamics by ERT
Srayeddin and Doussan, 2009	2-D ERT (32 electrodes), neutron probe and tensiometers	maize and sorghum / Avignon (France)	fully, moderately or poorly irrigation by sprinkler system	quantify RWU at different water supply levels
Boaga et al., 2013	3-D ERT (72 electrodes) and SW probes	apple orchard (full irrigated) / Maso Majano-Val di Non, Trento (Northern Italy)	drip and sprinkler irrigation	test the capabilities of small-scale ERT in monitoring eco-hydrological processes at the scale of interest for SPA interaction
Brillante et al. 2015	2-D ERT (24 electrodes), stem water potential measurements, and SW probes	vineyards / Aloxe-Corton, Burgundy (France)		monitor plant/- soil water relationships by ERT
Cassiani et al. 2015	3-D ERT (72 electrodes), ET from eddy covariance, sap flow data, and SW probes	orange orchard / Lentini, Sicily region (South Italy)	full drip irrigation	study the feasibility of small-scale monitoring of root zone processes using time-lapse 3-D ERT, ancillary data, and a physical-hydrological model; interpret data using a physical-hydrological model, and derive information on root zone physical structure and its dynamics
Moreno et al. 2015	2-D ERT (96 electrodes), SW and soil temperature probes	orange orchard (full irrigated) / Hadera, Israel	full drip irrigation	monitor root zone dynamics in a semiarid region using ERT
Satriani et al. 2015	2-D ERT (48 electrodes), ground penetrating radar,	dry bean crop / Basilicata Region, (Southern Italy)	no irrigation, intensive and economical drip irrigation	characterize crop roots following different irrigation treatments by ERT

	and SW probes			
Mares et al. 2016	2-D ERT (63 electrodes), sap flow measurements and SW probes	ponderosa pine / Boulder (Colorado)		evaluate application of ERT to identify high-resolution spatial and temporal changes in soil and tree water content
Cassiani et al. 2016	3-D ERT (72 electrodes) and SW probes	apple orchard (full irrigated) / Maso Majano - Val di Non, Trento (Northern Italy)	drip and sprinkler irrigation	test capabilities of small-scale ERT to monitor eco-hydrological processes at the scale of interest for SPA interaction; assess value of unsaturated flow modelling in supporting and validating the conclusions of time-lapse hydro-geophysical monitoring
Whalley et al., 2017	2-D ERT (96 electrodes), electromagnetic induction, soil water content (neutron probe), and soil strength (penetrometer).	23 types of winter wheat, two soil types, Woburn, UK.	no irrigation.	compare methods for phenotyping wheat lines
This study	3-D ERT (204 electrodes), sap flow measurements, SW and soil temperature probes	orange orchard / eastern Sicily (South Italy)	full drip irrigation and PRD technique	verify reliability of small scale ERT to qualitatively monitor soil-root interactions in two different irrigation treatments (full drip irrigation and partial root-zone drying); identify active RWU patterns for the two treatments, and their changes over time, by integrating time-lapse ERT with ancillary measurements

Table 2: Electrical conductivity (EC, dS m^{-1} 25°C) of the irrigation water from samples at the wells, samples at the drip lines, and the soil pore water solution extracted by suction cups in July and September 2015.

Monitoring period	**EC, dS m^{-1} (25°C)**		
2015	**Soil pore water**	**Water sampled from wells**	**Water emitted by the drip lines**
July	3.03 ± 0.52	2.16 ± 0.20	2.68 ± 0.39
September	1.79 ± 0.11	1.60 ± 0.07	1.72 ± 0.08

Table 3: Accuracy and resolution of the sensors used in the present study.

Sensor	Accuracy	Resolution
ECH_2O, Decagon Inc.	±1-2% Volumetric Water Content (VWC) with soil specific calibration	0.1% VWC
TVAC, Campbell Sci.	±0.2%	-25° to 50°C
Tranzflo NZ Ltd., Palmerston North, NZ	±0.2%	0.01 cm hr^{-1}
HD2106.2, delta OHM Italy	± 0.5% ± 1digit	5 µS/cm – 200 mS/cm

Table 4: Summary of total absolute inversion for 8-10 Jun, 14-17 Jul, and 21-24 Sep for T1 and T2 and an absolute inversion error of 16%.

Survey	Treatment	Dataset characteristics	No. of iterations to converge	Initial no. of measurements	Time for calculation (s)	No. of rejected measurements	RMS
8-10 Jun 2015	T1	background	5	2077	6173	526	1.78
	T2	background	4	2043	5038	349	1.88
14-17 Jul 2015	T1	background	4	3695	11355	659	1.24
		after irrigation	4	3501	8284	609	1.12
	T2	background	5	3590	6027	717	1.06
		after irrigation	6	2833	7105	529	1.14
21-24 Sep 2015	T1	background	4	4067	10606	1024	1.21
		after irrigation	4	4408	10574	875	1.23
	T2	background	5	3342	11591	1001	1.17
		after irrigation	4	2900	5633	462	1.12

Table 5: Times of ERT data acquisition at the different quarters, and irrigation schedules for T1 and T2.

Treatment	Acquisition	Starting time (GMT + 2)	Ending time (GMT + 2)	Irrigation schedule (GMT + 2)	Date
T1	time 00	8.30	8.55	9.00 – 12.00	July 15, 2015
	time 01	9.36	9.51		
	time 02	10.29	10.54		
	time 03	13.33	13.58		
T2	time 00	7.15	7.40	7.45 – 9.55	September 24, 2015
	time 01	8.37	9.02		
	time 02	9.16	9.41		
	time 03	12.27	12.52		

Figure1

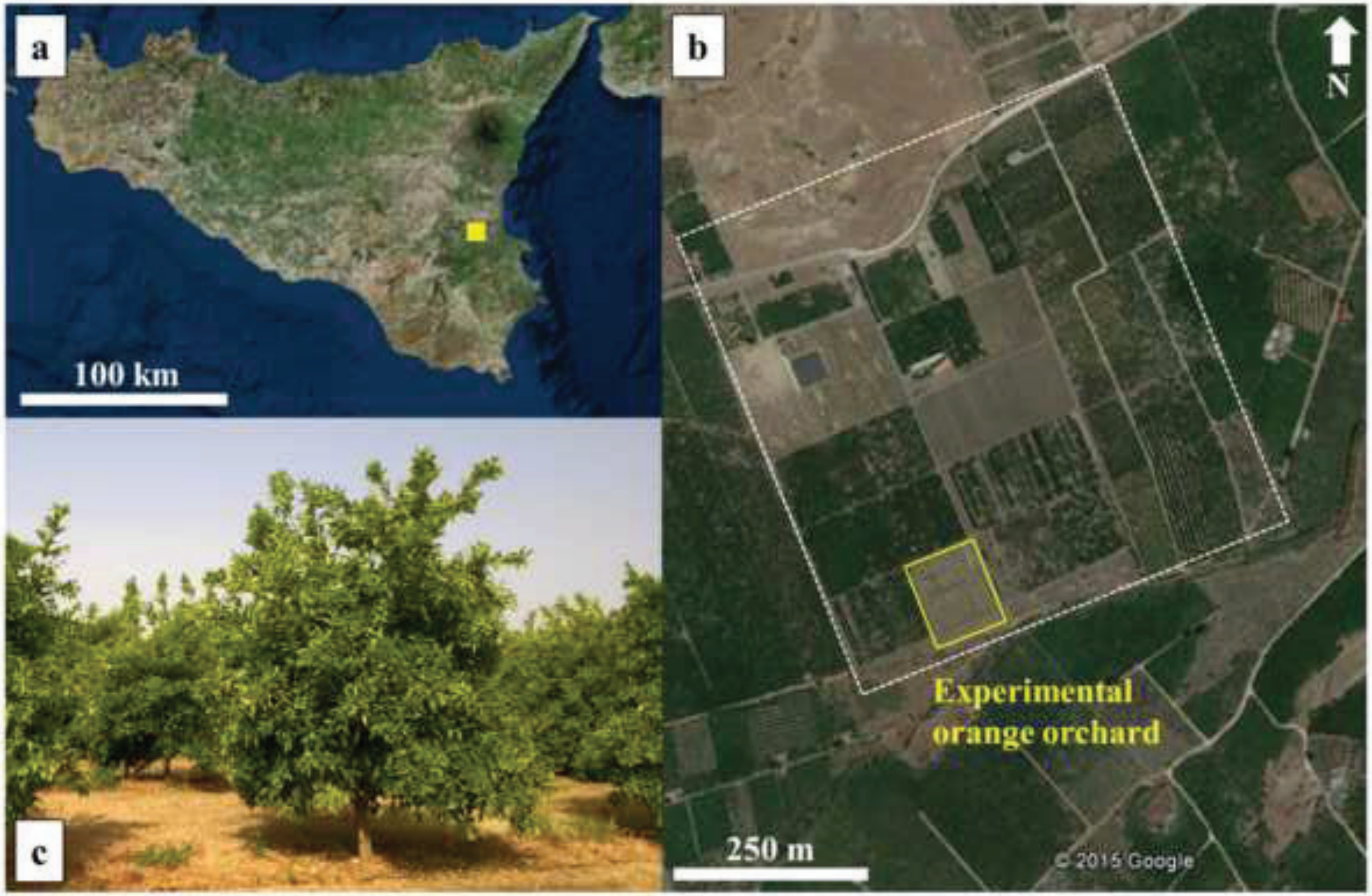

Figure2
Click here to download high resolution image

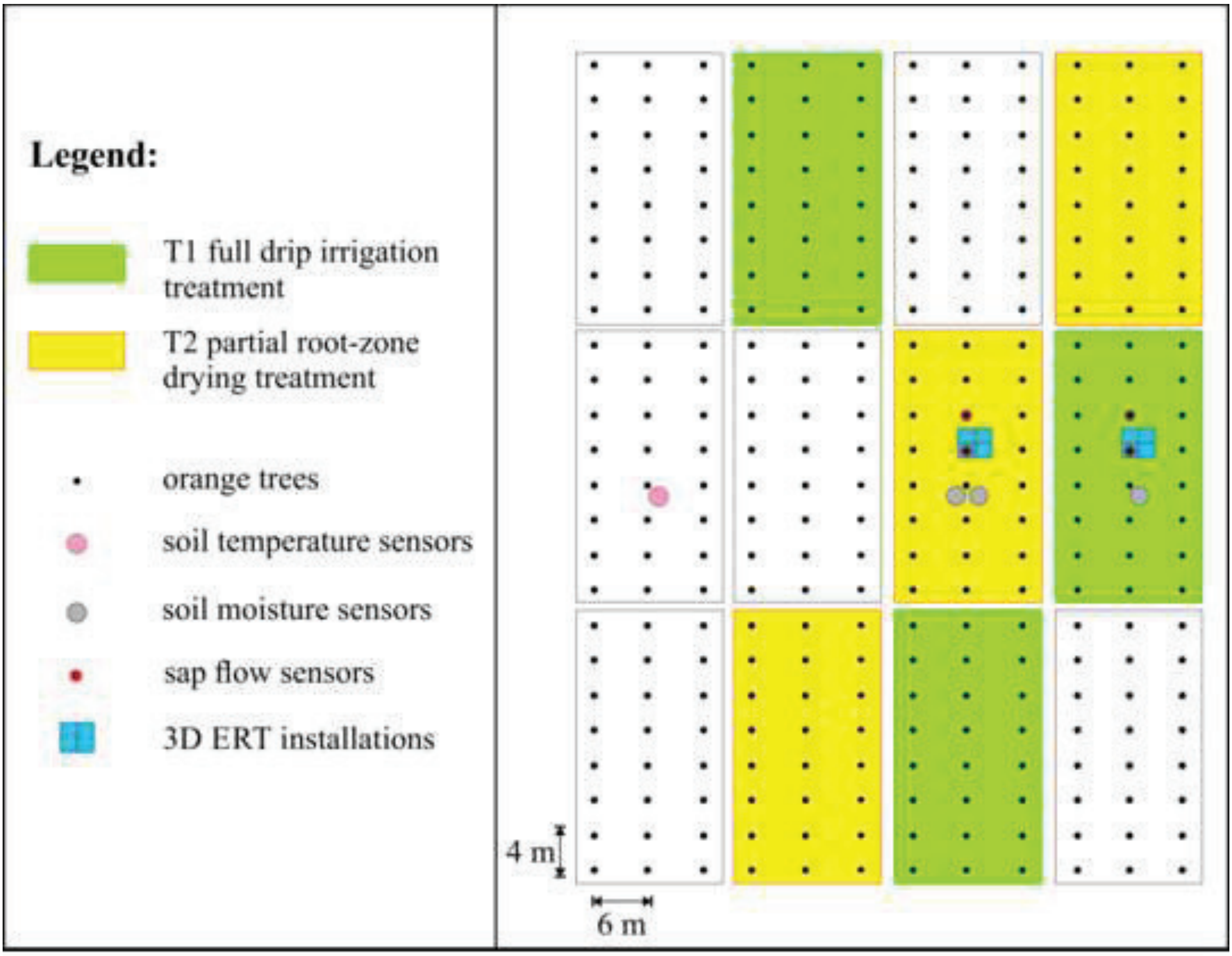

Figure3

Click here to download high resolution image

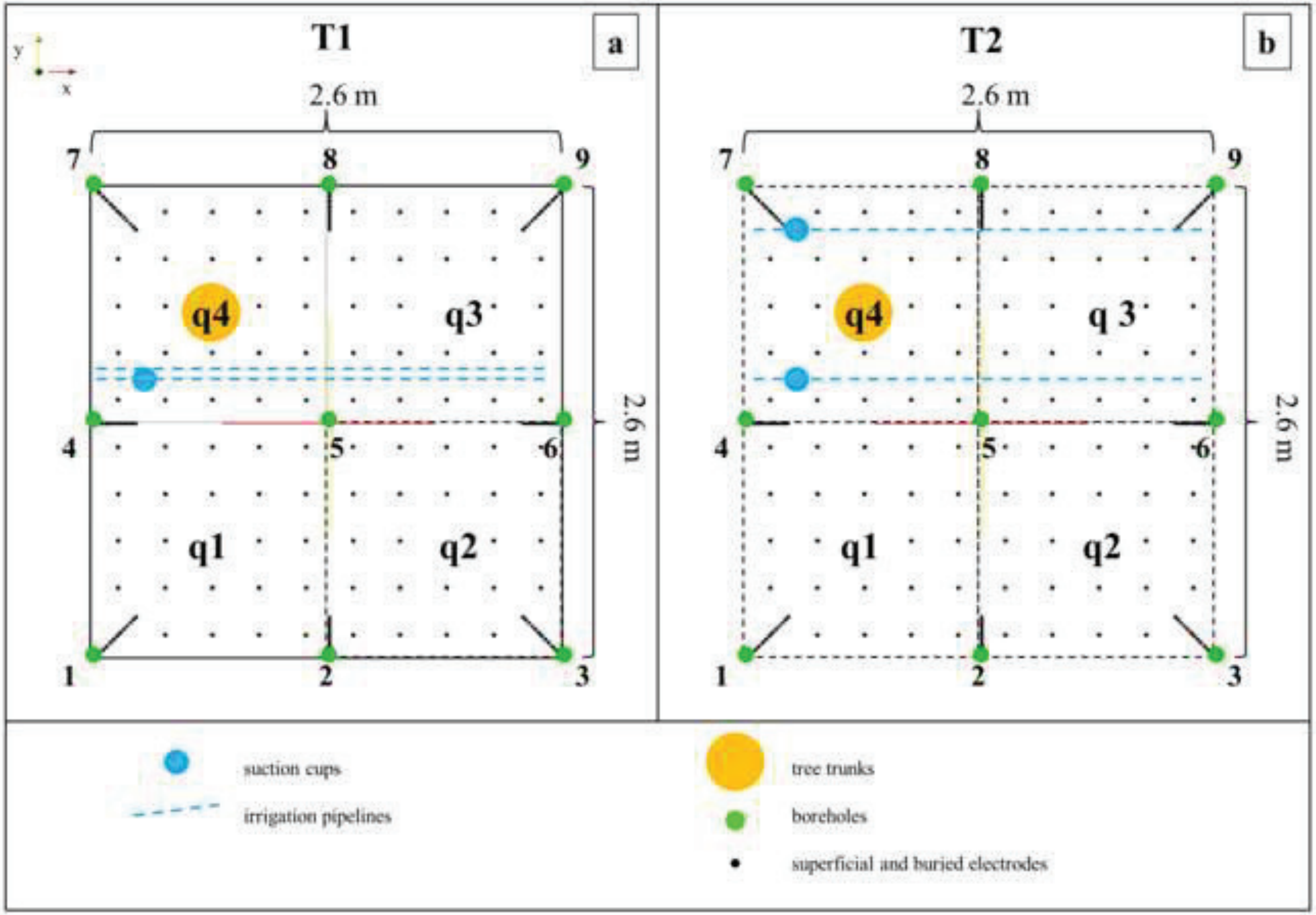

Figure4

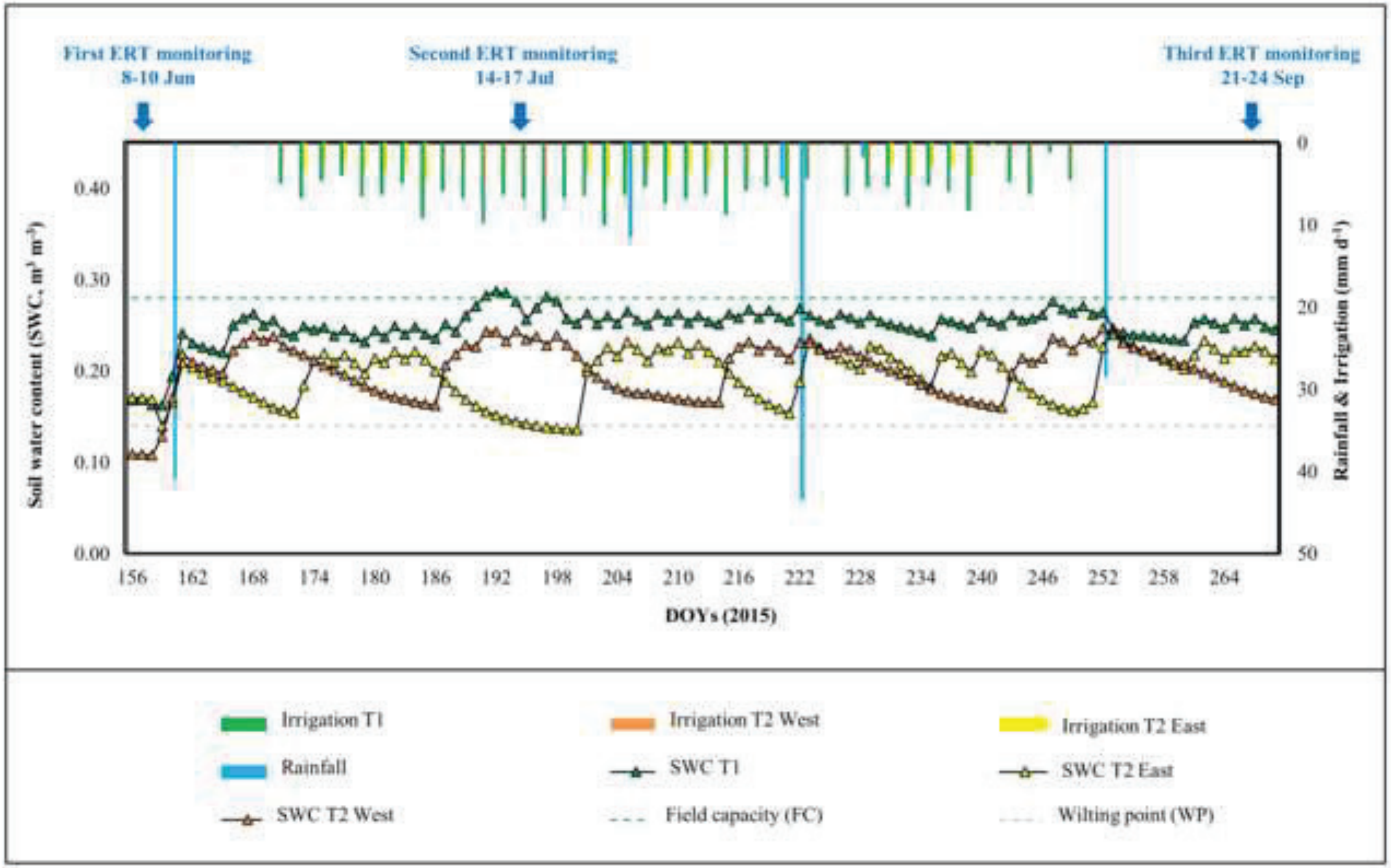
First ERT monitoring
8-10 Jun
Second ERT monitoring
14-17 Jul
Third ERT monitoring
21-24 Sep
Soil water content (SWC, m³ m⁻³)
0.40
0.30
0.20
0.10
0.00
Rainfall & Irrigation (mm d⁻¹)
0
10
20
30
40
50
156
162
168
174
180
186
192
198
204
210
216
222
228
234
240
246
252
258
264
DOYs (2015)
Irrigation T1
Irrigation T2 West
Irrigation T2 East
Rainfall
SWC T1
SWC T2 East
SWC T2 West
Field capacity (FC)
Wilting point (WP)

Figure5

Click here to download high resolution image

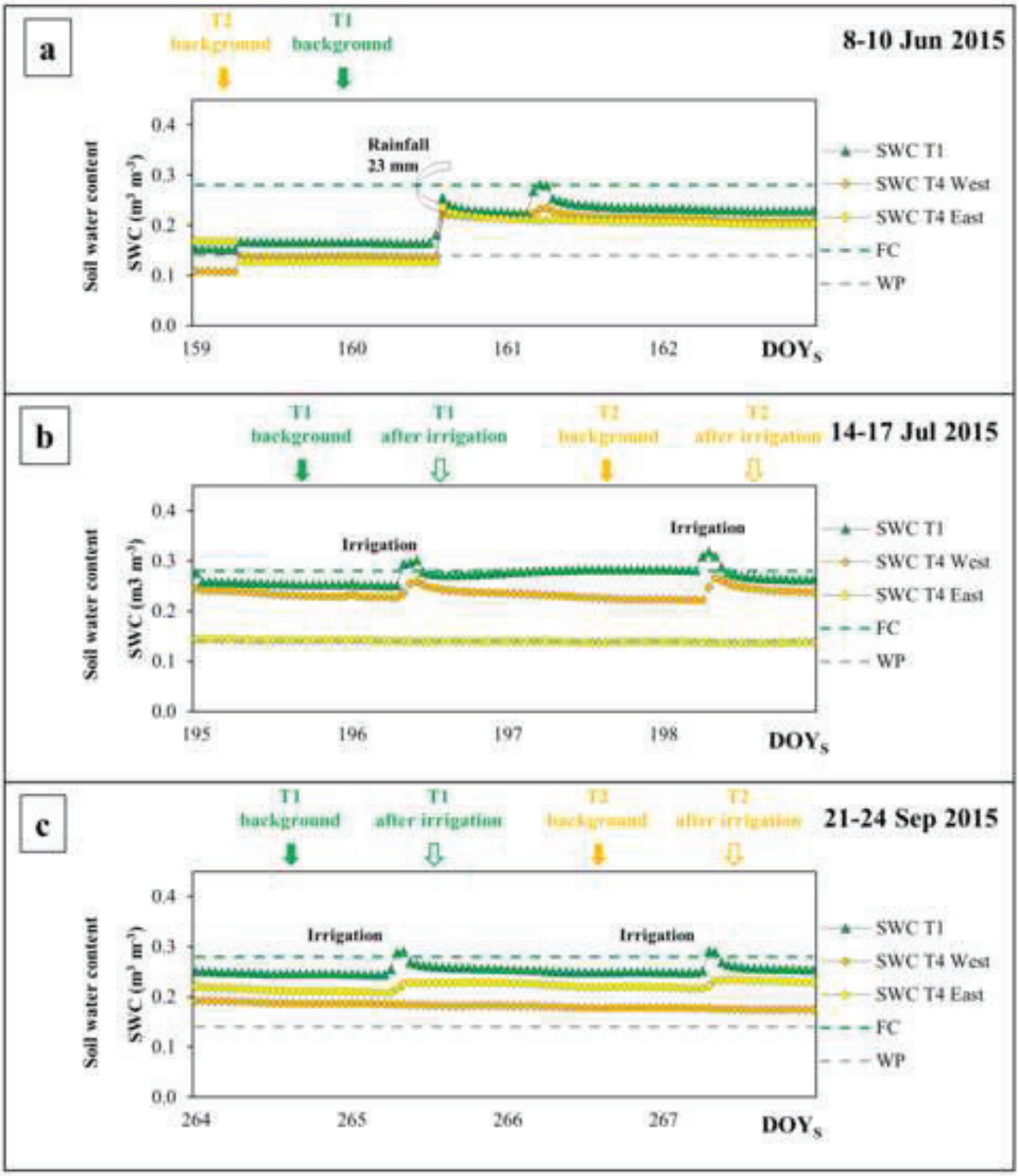

Figure6

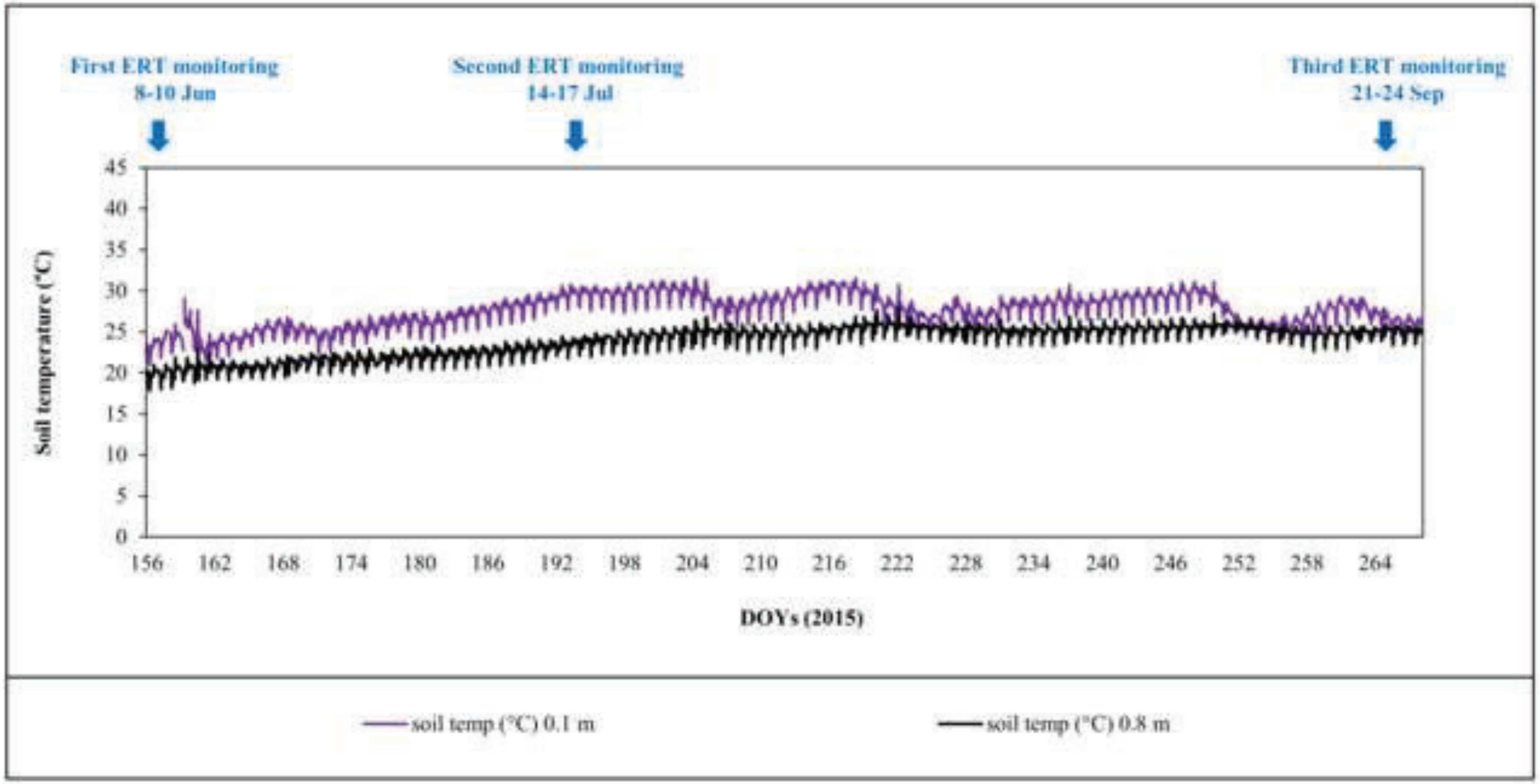
First ERT monitoring
8-10 Jun
Second ERT monitoring
14-17 Jul
Third ERT monitoring
21-24 Sep
Soil temperature (°C)
45
40
35
30
25
20
15
10
5
0
156
162
168
174
180
186
192
198
204
210
216
222
228
234
240
246
252
258
264
DOYs (2015)
soil temp (°C) 0.1 m
soil temp (°C) 0.8 m

Figure7
Click here to download high resolution image

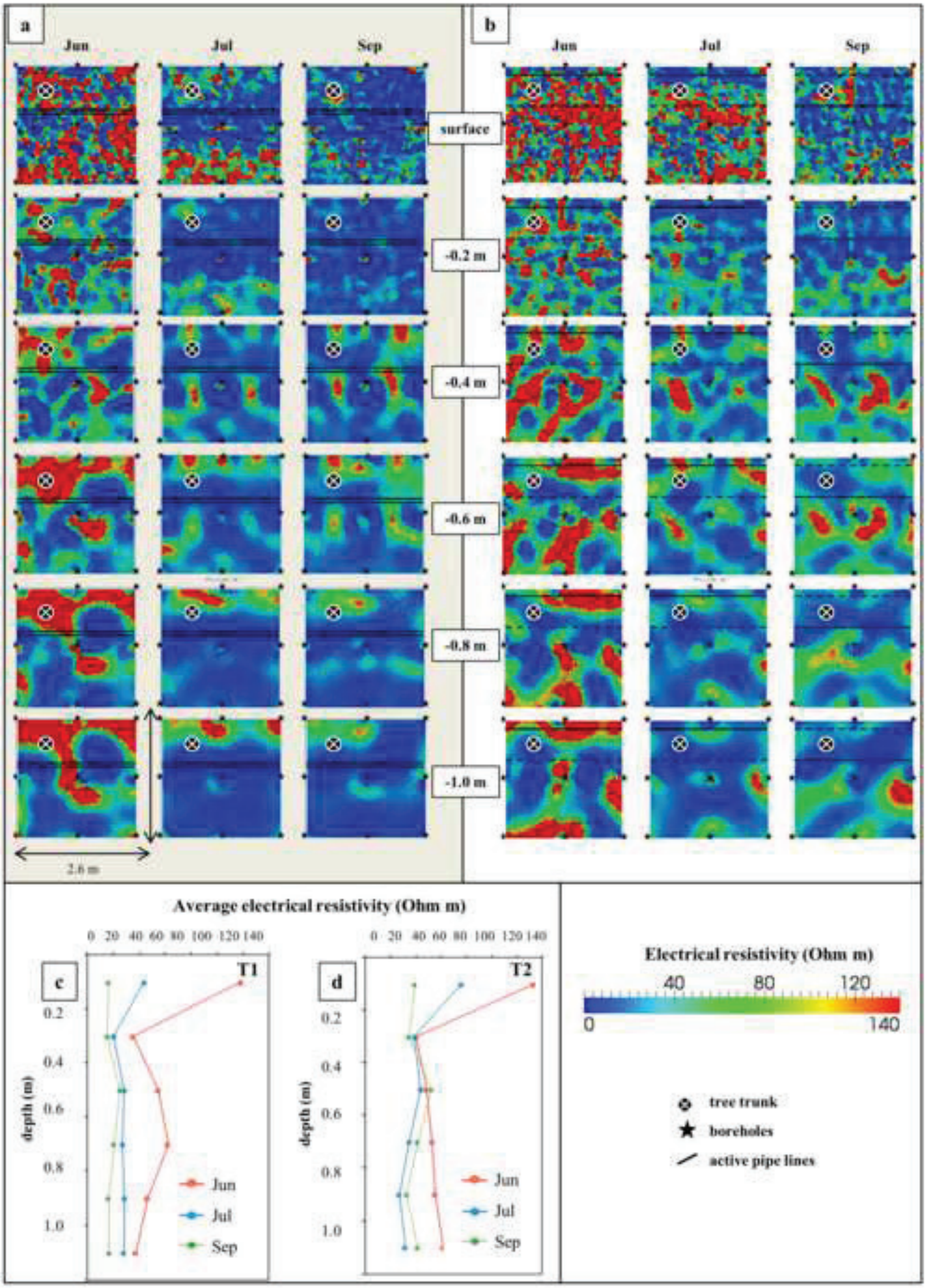

Figure8

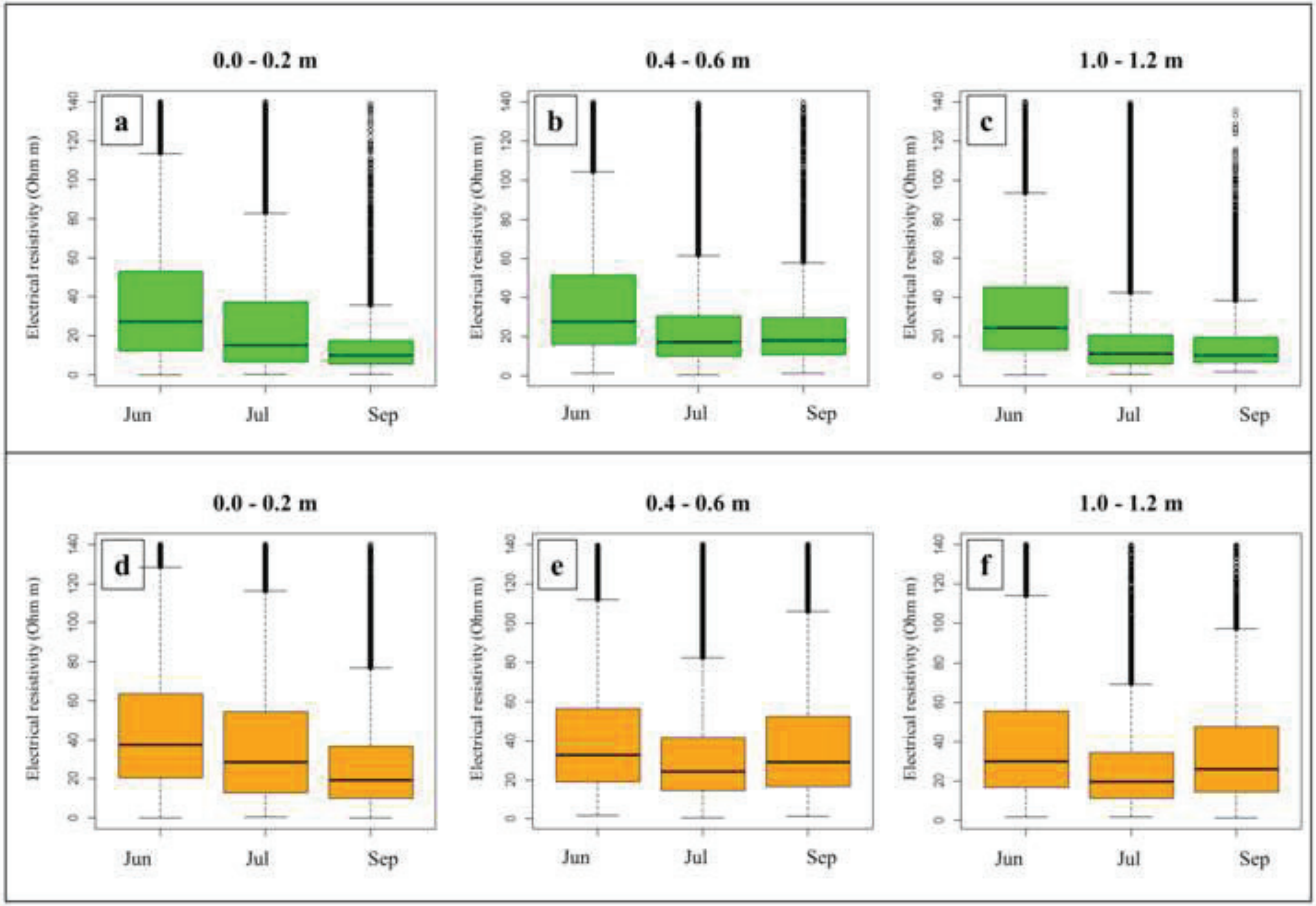

0.0 - 0.2 m
0.4 - 0.6 m
1.0 - 1.2 m
a
b
c
d
e
f
Electrical resistivity (Ohm m)
0
20
40
60
80
100
120
140
Jun
Jul
Sep

Figure9
Click here to download high resolution image

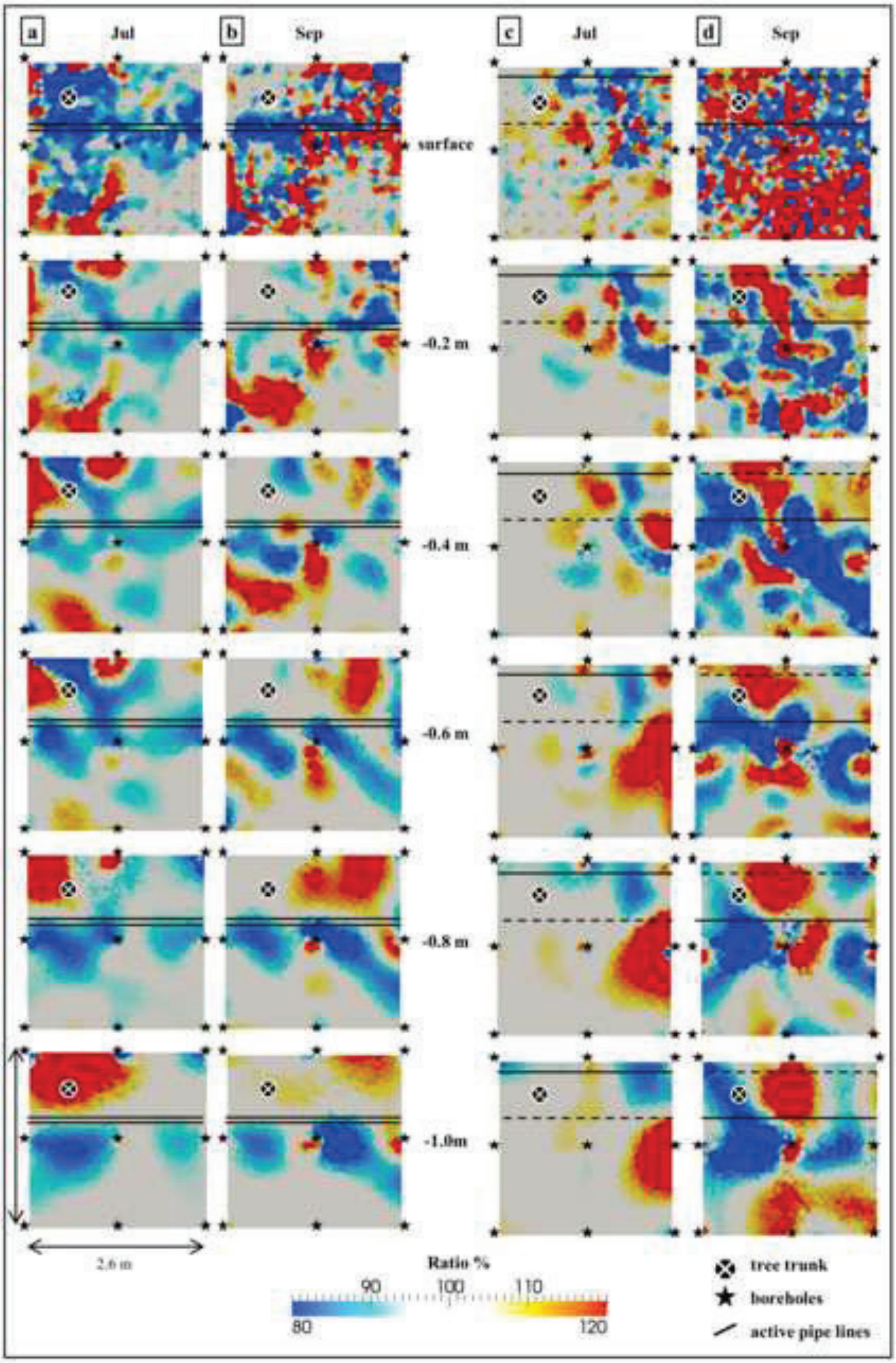

Figure10
Click here to download high resolution image

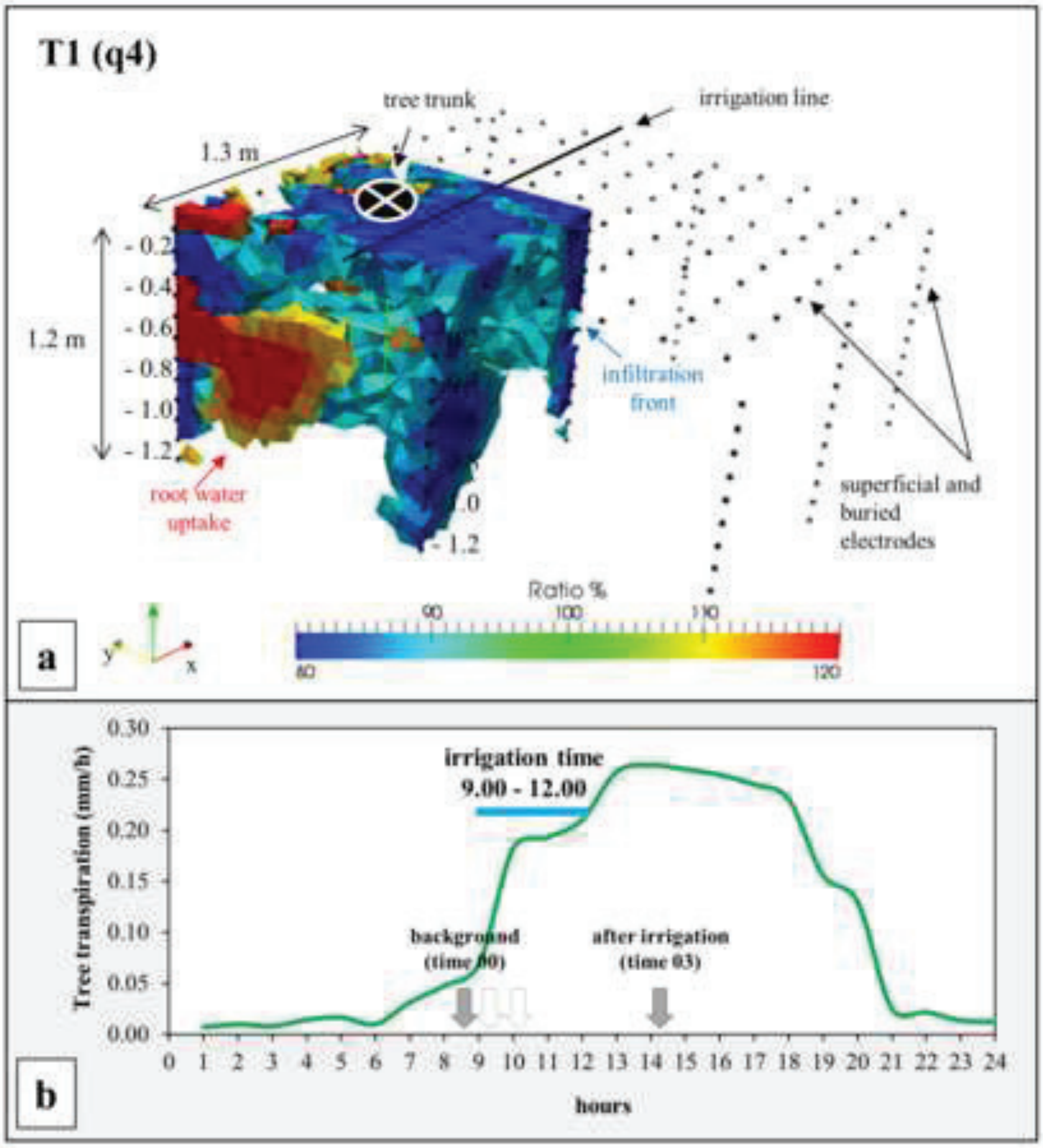

Figure11
Click here to download high resolution image